Journal of Infrared, Millimeter, and Terahertz Waves (2025) 46:50
https://doi.org/10.1007/s10762-025-01065-5

RESEARCH

ROCK: A Flexible Gyrotron Cavity Simulation Toolkit Using an Accuracy-Improved Time-Dependent Self-Consistent Multimode Interaction Model

Chuanren Wu[1] · Lukas Feuerstein[1] · André Schmidt[1] · Stefan Illy[1] · Manfred Thumm[1] · John Jelonnek[1]

Received: 13 March 2025 / Accepted: 24 June 2025

Abstract
Relativistic oscillator calculation kit (ROCK) is a self-consistent time-dependent multimode multi-harmonic code recently developed at KIT to simulate the interaction between electrons and microwaves in gyrotron cavities. Its key features include a flexible software design, the use of the finite element method, the capability for precisely resolving the electron motion, and an enhanced formulation of field excitation. The last two features are essential model differences and are discussed in detail. Preliminary simulation comparisons demonstrate the validity and highlight the potential advantages of the improved model implemented in ROCK.

Keywords Gyrotron · Cavity · Resonator · High-power microwaves · Electron cyclotron resonance · Beam-wave interaction · Nuclear fusion · Plasma heating

1 Introduction

Gyrotrons are vacuum electron tubes generating high-power microwaves (hereafter referred to as RF). Applications of gyrotrons can be found in magnetically confined fusion facilities and *dynamic nuclear polarization* (DNP) *nuclear magnetic resonance* (NMR) spectroscopy. The principle of a classical gyrotron is briefly explained as follows. The electron gun injects an annular hollow electron beam with a typical kinetic energy of up to 100 keV into a *cavity*. The cavity is a section of circular *waveguide* with carefully designed radial profile to facilitate beam-field interaction. Typically, the Larmor radius of the *electron cyclotron* (EC) orbit is smaller than the radius of the annular beam. The electrons of the annular beam follow helical cyclotron trajectories because of the static guiding magnetic field, which is significantly stronger than the RF and environmental magnetic field. The guiding magnetic field also defines

✉ Chuanren Wu
wu@kit.edu

[1] Karlsruhe Institute of Technology, Kaiserstr. 12, 76131 Karlsruhe, Germany

Published online: 11 July 2025

the electron cyclotron frequency of non-relativistic electrons. Considering relativity, the EC angular frequency is

$$\Omega_{\mathrm{e}} := -\frac{q_{\mathrm{e}}\, B_{\mathrm{sz}}}{\gamma\, m_0}\ , \tag{1}$$

where the subscript of B_{sz} means the static z component, as the dominant component of the total $\boldsymbol{B}$ field; γ is the Lorentz factor; and q_{e}/m_0 is the ratio of the electron charge to the electron rest mass. The beam exchanges energy along the cavity mainly with high-order *transverse electric* (TE) modes. After leaving the interaction region, the RF field may be converted to the linearly polarized fundamental Gaussian mode and launched outwards through the dielectric vacuum window, while the depleted electrons are collected.

Intensive simulations are required for designing and parametrizing a gyrotron, as well as for supporting the experiments. Usually, each component of a gyrotron is simulated individually, since distinct physical principles are involved. Among them, the modeling of cavities requires the Helmholtz equation for the RF field, the Poisson equation for the potential depression by the electron beam space charges, Lorentz force, and Newton's law of motion for the electron kinetics. As the geometrical size is much larger than the wavelength, reasonable assumptions and special techniques have to be applied for reducing the simulation time to a practical range [1–3]. The classical approaches in SELFT [4], TWANG [5], EURIDICE [6], and other similar codes not only compute quickly but also provide acceptable accuracy, as has been historically validated by experiments.

In this article, we present the essential improvements of the model implemented in the *relativistic oscillator calculation kit* (ROCK) recently developed at KIT. The basic version of ROCK implements a variant of the time-dependent self-consistent model, incorporating multimode and multi-harmonic interactions from the beginning. The differences of the methods in ROCK to the other codes of the same type are described in Section 2. Demonstrations in Section 3 show that ROCK produces results similar to classical codes, and its simulations are more accurate than existing codes of the same type in certain scenarios.

2 Similarities and Differences Compared to Codes of the Same Type

In this section, only the standard quasi-stationary model in ROCK is presented, with the discussion of the dynamic model reserved for future work. The quasi-stationary model of ROCK is compared with those of EURIDICE [6, 7] and SELFT [4], because the three codes used at KIT belong to the same category and share many common characteristics. ROCK incorporates some straightforward features that require no detailed explanations, such as follows:

- The used finite element (Galerkin) method allows for non-equidistant grid and local grid refinement.
- The mode carrier phases are independent, allowing for non-coherent mode competitions.

– High-order analytical and numerical terms are included. For example, the higher-order analytical term $S^{(1)}_{\mathrm{k,s}}$, which follows $S^{(0)}_{\mathrm{k,s}}$ in Eq. 13, is incorporated into the code implementation; Eqs. 8 and 9 include second-order numerical terms for advancing time and cyclotron phase, respectively.
– The software architecture is highly flexible and extendable. ROCK is not an executable binary blob; rather, it is a toolkit consisting of individual functions at fine granularity, featuring bindings to C99, Python, and MATLAB Simulink. Users can easily compose a program by combining these functions to solve non-standard problems, couple with thermal and mechanical co-simulations, integrate into optimizers, and swap these functions with their GPU counterparts.

The most significant differences from the classical time-dependent self-consistent fast-calculation model are as follows:

– The velocities and positions of electrons in ROCK are strictly resolved. Their correctness is verifiable (e.g., as unit-tests) using solutions calculated in Cartesian coordinates.
– Multiple harmonic terms are considered in the Lorentz force, which further enhances the accuracy of the electron motion.
– The expression for field excitation has fewer approximations and can optionally include multiple harmonic terms as well.

As will be shown, these features of physical model can lead to higher accuracy that becomes observable in certain scenarios.

The interaction model in ROCK shares some common concepts with other classical codes to achieve comparable computational speed. One common assumption is the aforementioned quasi-stationary state. It means that within the characteristic time of field envelope evolution, the electron beam perceives the field as "frozen" and transits through the entire simulation region, experiencing different carrier phases of this "frozen" field envelope. On the other hand, the stationary field is approximately excited by a full single transit of electrons during each step of the envelope evolution. As speaking of envelope and carrier, the field of each waveguide mode is formulated as an amplitude modulation due to its assumed narrow frequency bandwidth. The narrowband envelope at the baseband can be resolved with temporal steps larger than those dictated by the Nyquist sampling limitation concerning the actual field (carrier) frequency. For this reason, the envelope is referred to as a *slow-varying* quantity in the literature. In addition to the field and its excitation source, the electron motion can also be transformed to a slow-varying formulation. Details are explained in the following subsections. However, rigorous mathematical definitions have been omitted because they do not add new insight to the field. Readers are suggested to consult textbooks, relevant reports [3, 4], other articles [6, 7], or the forthcoming monograph by the leading author for mathematically rigorous derivations.

2.1 Electron Motion

Before diving into the models, it is important to clarify the term "guiding center." Generally, the motion of guiding center is solved from the collection of all zero-order

terms in the expanded motion equation by Lorentz force. The particular solution of the guiding center equation is a field line of the dominating static magnetic field, which is referred to as the *ideal guiding center*. Secular effects of the high-order terms, in the presence of an RF field, may cause the *actual guiding center*,

$$\boldsymbol{r}_{\mathrm{g}\perp,\mathrm{actual}} = \frac{1}{2\,\pi} \oint \boldsymbol{r}_{\mathrm{e}\perp}\,\mathrm{d}\phi \tag{2}$$

to deviate slightly from the original magnetic field line, where $\boldsymbol{r}_{\mathrm{e}}$ is the electron position vector and ϕ is the cyclotron phase. This change of field line rarely affects the so-called coupling factor. However, maintaining an accurate description of electron motion, especially tracking the exact cyclotron phase relative to the field, becomes delicate if the guiding center is no longer ideal. It should be noted that Eq. 2 is not intended for direct evaluation; therefore, the actual guiding center is a rather vague concept. Lastly, the term *numerical guiding center* refers to the program's state variable.

This paragraph briefly summarizes the classical model for later comparisons. The key parameters of an electron's motion are its position and velocity. Let $\boldsymbol{u} := \gamma\,\boldsymbol{v}$ and i represent the imaginary unit. For convenience, $\boldsymbol{u}$ is also referred to as *velocity* in this article. The classical model uses a complex number to represent the *two-dimensional* (2D) vector $\boldsymbol{u}_\perp$. This complex representation facilitates the formulation of electron rotation as another amplitude modulation

$$u_\perp = u_{\perp,\mathrm{env}}(t)\ \exp\bigl\{\mathrm{i}\,\omega_{\mathrm{e}}(t - t_0)\bigr\} \tag{3}$$

(see Eq. (5) of [7] for example). Determining the vector $\boldsymbol{u}_\perp$ requires two quantities: its direction and magnitude. In cyclotron coordinates, the direction of $\boldsymbol{u}_\perp$ consists of the rotor phase $\omega_{\mathrm{e}}(t - t_0)$, plus the phase of its complex envelope $u_{\perp,\mathrm{env}}$ as a corrective angle. The magnitude $|\boldsymbol{u}_\perp|$ is given by the modulus $|u_{\perp,\mathrm{env}}|$, and it is treated as $|\boldsymbol{u}_\perp| = |u_\phi|$. To determine the position of an electron in cyclotron coordinates, three parameters are required: the cyclotron angle ϕ, the Larmor radius r_{L}, and the guiding center position. They are evaluated as follows: Transversally rotating the angle of velocity by 90° results in the ϕ angle; the Larmor radius is calculated using $r_{\mathrm{L}} = |v_\perp/\omega_{\mathrm{e}}|$ where the frequency of the slowly varying $u_{\perp,\mathrm{env}}$ can be safely ignored; the numerical guiding center corresponds to the ideal guiding center.

The model of electron motion in ROCK is different from the classical one. To avoid ambiguity between the i associated with the field and the i associated with space, the motion state in the following text is expressed using real vectors instead of complex phasors. Although the final formulae for the Lorentz force are equivalent, this equivalence is not generally guaranteed, as will be discussed in the subsection on field excitation. Similar to the complex formulation, the components of cyclotron velocity are slowly varying, as far as the numerical guiding center position $\boldsymbol{r}_{\mathrm{g}}$ and the numerical local angular frequency ω_{e} are properly determined. Sorting and collecting terms by their basis vector from the complete equation of Newton's second law yield more organized expressions:

$$\frac{m_0}{q_{\mathrm{e}}}\begin{bmatrix} u'_\phi \\ u'_{\mathrm{L}} \end{bmatrix} = \frac{1}{v_z}\begin{bmatrix} E_\phi \\ E_{\mathrm{L}} \end{bmatrix} + \begin{bmatrix} B_{\mathrm{L}} - \frac{r_{\mathrm{L}}}{2} B'_{\mathrm{sg}z} \\ -B_\phi \end{bmatrix} + \bigl[B_{\mathrm{w}z} + B_{\mathrm{sg}z}\,(1 - \tilde{\omega})\bigr]\begin{bmatrix} -\alpha_{\mathrm{L}} \\ \alpha_\phi \end{bmatrix} \tag{4}$$

$$\frac{m_0}{q_\mathrm{e}}\,u_z' = \frac{E_{\mathrm{s}z}}{v_z} - \alpha_\phi\,\left(B_\mathrm{L} - \tfrac{r_\mathrm{L}}{2}\,B_{\mathrm{sg}z}'\right) + \alpha_\mathrm{L}\,B_\phi - \frac{v_{\mathrm{g}\theta}}{v_z}\,B_{\mathrm{sg}r}\ . \tag{5}$$

The reader may compare these expressions with Eq. (3.55) of [4]. The conventions used in these equations are explained as follows: Let θ be the azimuthal angle, z the axial coordinate, and z_e the axial position of an electron. The prime symbol ($'$) designates the derivative $\mathrm{d}/\mathrm{d}z_\mathrm{e}$. Subscript "$_\phi$" and "$_\mathrm{L}$" indicate the two perpendicular components of a vector projected onto the cyclotron coordinates, where "$_\mathrm{L}$" stands for the direction of Larmor radius, i.e., $\boldsymbol{r}_\mathrm{L} := \boldsymbol{r}_\mathrm{e} - \boldsymbol{r}_\mathrm{g}$. The italic r designates a radius, while the bold sans-serif $\boldsymbol{r}$ designates a position vector. The terms $\alpha_\phi := u_\phi/u_z$ and $\alpha_\mathrm{L} := u_\mathrm{L}/u_z$. The subscripts in $B_{\mathrm{sg}z}$ indicate the z component of the static field at the guiding center. $B_{\mathrm{w}z}$ represents the RF B_z at $\boldsymbol{r}_\mathrm{e}$, where the subscript "$_\mathrm{w}$" stands for wave. The term $\tilde{\omega} := \omega_\mathrm{e}/\,\Omega_\mathrm{e}$ serves as the figure-of-merit for the eccentricity, which is integrated by

$$\frac{\tilde{\omega}'}{\tilde{\omega}} = \frac{u_\phi'}{u_\phi} - \frac{B_{\mathrm{sg}z}'}{B_{\mathrm{sg}z}} - \frac{\alpha_\mathrm{L}}{r_\mathrm{L}}\ . \tag{6}$$

It is to note that ω_e is handled differently than in Eq. (16) of [7]. Ideally, $\tilde{\omega} = 1$. If at any point $\tilde{\omega}$ deviates significantly from 1, it indicates that the numerical guiding center may no longer be appropriate for assuming the validity of slowly varying quantities. However, results using an improper numerical guiding center can still be accurate if the step length is decreased. When this occurs, ROCK calibrates the numerical guiding center using the static B-field, resetting $\tilde{\omega}$ to 1, u_L to 0, and u_ϕ to $u_\perp$, without affecting the actual position and velocity from a perspective neutral to the coordinate system. In this article, the local coordinates are still referred to as "cyclotron coordinates," even though the coordinate basis vectors and the numerical guiding center (the origin of the coordinates) do not necessarily reflect the actual physical values associated with cyclotron motion. Hence, the state vector of an electron contains eight components as function of z:

$$\text{state} := (t\ \ \phi\ \ \tilde{\omega}\ \ \alpha_\mathrm{L}\ \ \alpha_\phi\ \ u_z\ \ r_\mathrm{g}\ \ \theta_\mathrm{g})^\mathrm{T}\ . \tag{7}$$

If the static B-field is axisymmetric, the component r_g for the guiding center radius can be replaced by the magnetic flux enclosed by a centered transverse circle, taking the aforementioned eccentricity correction into account. In the state vector, the other components, except for t and ϕ, are slowly varying and can be calculated using relatively large steps. Therefore, numerical steps of t and ϕ include additional terms in the order of δz^2 to enhance their convergence:

$$\delta t = \left\{ \frac{1}{v_z}\,\delta z + \frac{\left(\alpha_\phi'\,\alpha_\phi + \alpha_\mathrm{L}'\,\alpha_\mathrm{L}\right)\,(u_z/c_0)^2 - u_z'/u_z}{2\,\gamma\,u_z}\,\delta z^2 + \cdots \right\}_{z=z_\mathrm{start}} \tag{8}$$

$$\delta\phi = \left\{ \frac{\alpha_\phi}{r_\mathrm{L}}\,\delta z + \frac{1}{2}\left(\frac{\alpha_\phi'}{r_\mathrm{L}} - \frac{\alpha_\phi}{r_\mathrm{L}}\,\frac{\alpha_\mathrm{L}}{r_\mathrm{L}}\right)\delta z^2 + \cdots \right\}_{z=z_\mathrm{start}} \tag{9}$$

where the preceding δ denotes differences associated with each step of the electron's motion. At a higher level, the entire state vector is advanced using the predictor-corrector method to approach global second-order convergence.

Another highlight of the ROCK model is its incorporation of multiple harmonic terms from the field expansion to enhance the accuracy of electron motion. The transformation from cylindrical coordinates to cyclotron coordinates utilizes Graf's generalization of Neumann's addition theorem, as detailed in Chapter 11.3 of [8]. This transformation does not require the numerical guiding center to coincide with the actual one. The addition theorem yields a series with an integer index "$\mathtt{s}$," which can be physically interpreted as the harmonic number of interaction. For example, the total field applied into Eq. 4 consists of $E_\phi = \sum_\mathtt{k} E_{\phi,\mathtt{k}}$ and $E_\mathrm{L} = \sum_\mathtt{k} E_{\mathrm{L},\mathtt{k}}$ where $\mathtt{k}$ is an integer indicating a mode from the simulated mode list. The electric field components of the $\mathtt{k}$'th mode should be evaluated from the series

$$E_{\phi,\mathtt{k}} = \sum_{\mathtt{s}=-\infty}^{+\infty} E_{\phi,\mathtt{k},\mathtt{s}} \quad \text{and} \quad E_{\mathrm{L},\mathtt{k}} = \sum_{\mathtt{s}=-\infty}^{+\infty} E_{\mathrm{L},\mathtt{k},\mathtt{s}} \tag{10}$$

In classical codes, only a single $\mathtt{s}$ is considered for each mode. In contrast, ROCK considers $\mathtt{s} \in \{0, 1, 2, 3\}$ by default. This default range suffices to include both the fundamental (first harmonic) and second-harmonic interactions, while providing additional correction and margin by also incorporating $\mathtt{s} = 0$ and $\mathtt{s} = 3$. The range of $\mathtt{s}$ is a compile-time variable, offering sufficient flexibility while aiding the compiler in unwrapping and vectorizing the corresponding loops.

A simulation step of the cavity in [9] is performed to demonstrate the effect of incorporating multiple harmonic terms. A fixed RF field with output power of 200 kW

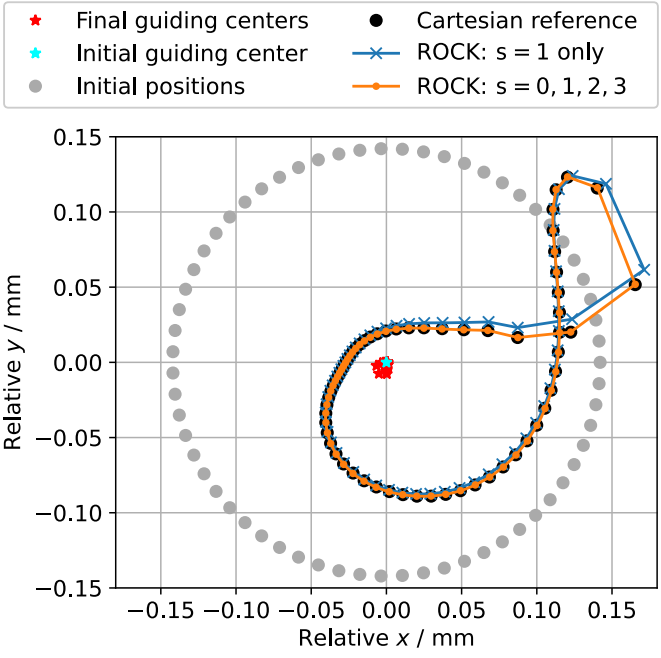

Fig. 1 Positions of electrons at the end of the cavity

is manually established, whose frequency and envelope matches the ones of its cold resonance. A probe beam represented by 63 electrons evenly distributed around the same initial guiding center is injected into the cavity. Being compared are the positions of electrons when they are leaving the cavity. For reference, the positions calculated using the Boris [10] or Buneman [11] method in Cartesian coordinates are presented. Figure 1 shows that considering multiple harmonic terms further enhances the accuracy of electron motion. Moreover, stronger interactions tend to exhibit more significant differences, especially when certain electrons bunch and drift extensively, crossing their original guiding centers.

Upon comparing both models, it becomes apparent that the classical model significantly simplifies the situation by assuming $u_\perp = u_\phi$ and anchoring the numerical guiding center to a field line. This was a clever simplification: although the state of a single electron may not be accurately represented, the model performs well statistically in terms of energy exchange for an ensemble of electrons in standard scenarios. In contrast, the ROCK model has the capability to integrate position and velocity accurately while maintaining a similar computational speed by also utilizing slow variables.

2.2 Field Excitation

In the transformed Helmholtz equation, the source term used to excite a TE-mode is denoted by the symbol "S" in the following text. Its physical formulation with respect to the slow-varying amplitude-modulated field is

$$S_{\mathrm{k}} := 2\,\mu_0\, e^{-\mathrm{i}\,\omega_0\, t} \iint \mathfrak{e}^*_{\mathrm{k}} \cdot \frac{\partial \boldsymbol{J}_\perp}{\partial t}\, \mathrm{d}^2 r_\perp \tag{11}$$

where $\mathfrak{e}$ is the TE-mode eigenvector, k is an index of the considered mode list, μ_0 is the vacuum permeability, and ω_0 is the carrier frequency. Numerically, it is evaluated similar to Eq. 10 as

$$S_{\mathrm{k}} := \sum_{\mathrm{s}} S_{\mathrm{k,s}} \tag{12}$$

with $S_{\mathrm{k,s}}(z_{\mathrm{e}}) := S^{(0)}_{\mathrm{k,s}} + S^{(1)}_{\mathrm{k,s}} + \ldots$ whose dominating term is

$$S^{(0)}_{\mathrm{k,s}} = 2\,\mu_0 \sum_{\mathrm{i}}^{\text{traj.}} I_{z,\mathrm{i}}\, e^{-\mathrm{i}\,\phi_{0,\mathrm{k}}(z_{\mathrm{e,i}})}\, v_{z,\mathrm{i}} \left[\begin{pmatrix} \alpha'_\phi \\ \alpha'_{\mathrm{L}} \end{pmatrix}_{\mathrm{i}} + \mathrm{i}\,\mathrm{s}\, \frac{B_z}{|B_z|} \frac{\alpha_{\phi,\mathrm{i}}}{r_{\mathrm{L,i}}} \begin{pmatrix} \alpha_\phi \\ \alpha_{\mathrm{L}} \end{pmatrix}_{\mathrm{i}} \right] \cdot \begin{pmatrix} \mathfrak{e}^*_\phi \\ \mathfrak{e}^*_{\mathrm{L}} \end{pmatrix}_{\mathrm{k,s}} \tag{13}$$

where ϕ_0 is the carrier phase. The next-order term $S^{(1)}_{\mathrm{k,s}}$ is implemented in the program but not introduced in this article for the sake of conciseness. Equation 13 is similar to the formulation of SELFT (cf. Eq. (4.45) of [4]). One potential difference compared to some codes is the coefficient of the second term in Eq. 13, whose magnitude should be $v_z\,\alpha_\phi / r_{\mathrm{L}} = \omega_{\mathrm{e}} = \tilde{\omega}\,\Omega_{\mathrm{e}}$ instead of the approximation with $\omega_{0,\mathrm{k}}$ of the field. Another difference is in the incorporation of the term $(\alpha'_\phi\ \alpha'_{\mathrm{L}})$: both ROCK and SELFT take this term into account, whereas it was ignored in some analyses (e.g., [1, 7]) (see also [3, 4] for further discussions). When examining a single harmonic term, the primary feature

of ROCK is the use of vector form rather than a complex phasor. The vector form clearly distinguishes between multiplying by i and rotating the eigenvector by 90°. Moreover, the vector form results in slightly different calculations, where α_L should be multiplied with ϵ_L^*. Notably, ϵ_L^* and ϵ_ϕ^* have different magnitudes.

Similar to the calculation of the Lorentz force, Eq. 12 includes multiple harmonic terms by default. Its effect in a monomode simulation is demonstrated in Fig. 2. In this particular scenario, including multiple terms shows good agreement with the Cartesian reference within the up-taper section and may reveal further details of the after-cavity interaction. Generally, Eq. 12 is capable of handling cases where the harmonic ratio $\omega_0/\,\Omega_\mathrm{e}$ is not close to an integer, which may occur with parasite modes. The potential advantages of including multiple harmonic terms must be carefully justified in future investigations.

3 Demonstrations

This section presents two simulation examples to demonstrate the capabilities and improvements of the implemented model. The first, a $\mathrm{TE}_{28,16}$ coaxial cavity, is compared with the literature [4, 12] to validate standard scenarios. The second involves an idealized setup of a second-harmonic TE_{02} interaction and is compared against a full-wave *particle-in-cell* (PIC) code to highlight the differences from classical codes.

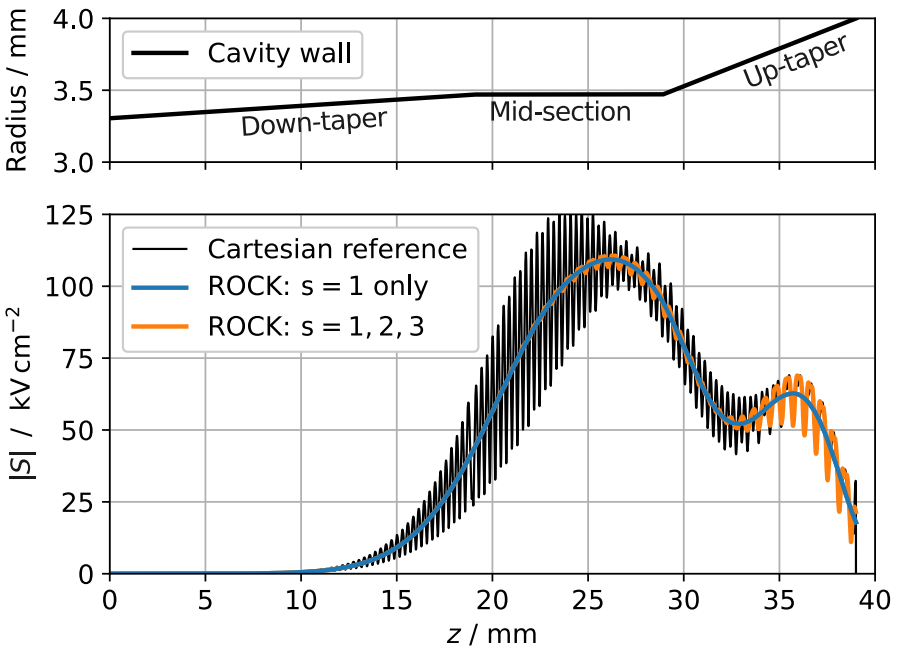

Fig. 2 RF excitation for the same setup which has produced Fig. 1. The case with $\mathrm{s} = 1$ includes multiple harmonic terms of the Lorentz force, too

Table 1 Comparison between ROCK and SELFT at the designed operating point

	P_{monomode}	f_{monomode}	$P_{\text{multimode}}$	$f_{\text{multimode}}$
ROCK	1.73 MW	139.967 GHz	1.64 MW	139.959 GHz
SELFT	1.72 MW	139.96 GHz	1.67 MW	139.96 GHz

3.1 Coaxial Cavity Operating in a High-Order Mode

The geometry of the simulated coaxial cavity is defined on page 182 of [4]. The quasi-stationary operating points for both mono- and multimode cases from Tab. 7.2 of [4] are referred. To achieve the hard-excitation operating point, the beam voltage U_b is ramped up from 75 to 90 kV, while the pitch factor α_ϕ and beam current I_b are scaled according to Chapter 5.3 of [13]. Further details on the operating point are given on page 184 of [4]. The results are compared in Table 1 and visualized in Fig. 3.

Both operating frequency and power at the designed operating point show very good agreement with the literature values. Furthermore, as discussed on page 188 of [4], the experiment of the gyrotron with this cavity showed a drop of the power in the operating mode $\text{TE}_{28,16}$ before losing the mode. This effect can be simulated in ROCK, as shown in Fig. 3. However, the reader should note that conducting an experimental comparison and analyzing uncertainties and error bars would require significant effort. A comprehensive experimental validation will be addressed in a separate article.

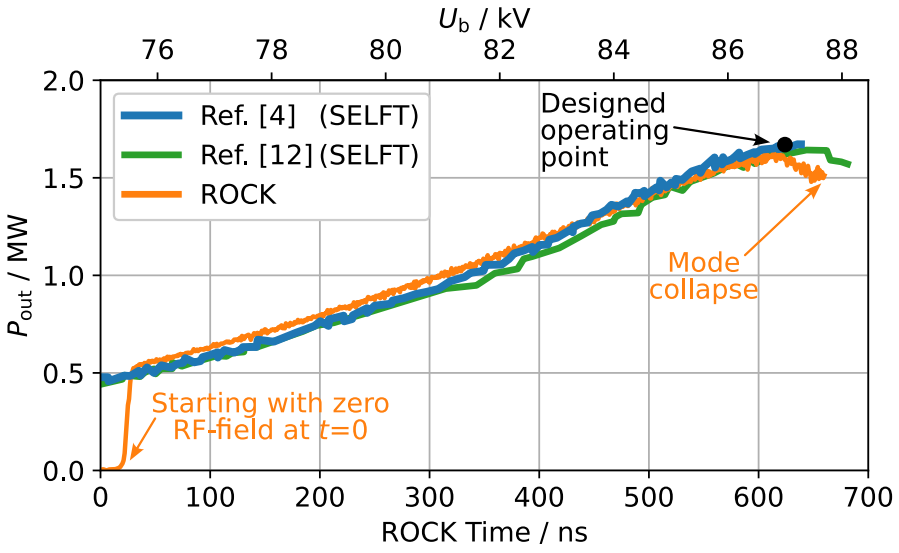

Fig. 3 Stable $\text{TE}_{28,16}$ operating regime from multimode calculations of the coaxial cavity

Table 2 Parameters of the demonstration case

Radius of mid-section	Down-taper	Mid-section	Up-taper
3.47 mm	30 mm 2.5°	32.5 mm 0°	30 mm 2°
Initial pitch factor	Beam current	Beam radius	Magnetic field
1.5	5 A	1.53 mm	1.92 T

3.2 Second Harmonic Cavity with Azimuthally Symmetric Modes

To furthermore investigate the improved model, a second-harmonic TE_{02} example is demonstrated in this section. The code EMPIC is used to provide reference values because it makes minimal assumptions aside from azimuthal symmetry. EMPIC, as part of the in-house beam-optics package ESRAY [14], is a full-wave PIC code incorporating the solution of Maxwell's equation on a 2D structured, non-orthogonal simulation mesh in cylindrical coordinates using the *finite-difference time-domain* (FDTD) scheme proposed by Holland [15]. The motion of the particles is computed numerically using the aforementioned Boris method, applied to three velocity components (v_z, v_r, v_θ) but only two spatial (z, r) components. Consequently, only the interaction with TE_{0n} modes are considered in the following comparison.

The cavity shape and beam parameters are defined in Table 2, which yields a resonance frequency of approximately 96.5 GHz for the second-harmonic main mode TE_{02}. The given beam parameters and the static magnetic field are kept constant for simplicity. Additionally, the space charge effect is disabled to eliminate differences in how the electrostatic effects are handled, ensuring that the comparison focuses solely on the interaction mechanism.

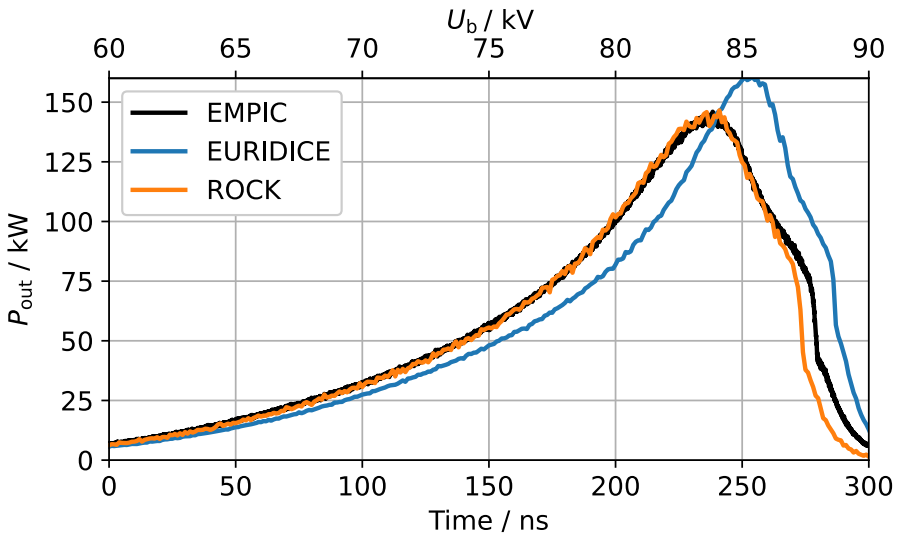

Fig. 4 Simulations of the second-harmonic cavity

Figure 4 presents the output power during the ramp-up of beam voltage from 60 to 90 kV within 300 ns. ROCK produces results very close to EMPIC, whereas EURIDICE exhibits a slight deviation in the power profile. Various combinations of options have been tested in EURIDICE, but this deviation persists. This comparison indicates that ROCK is more accurate in certain scenarios.

4 Conclusion

This article presents the model implemented in the recently developed gyrotron interaction code, ROCK. Differences from classical codes of the same type are discussed in detail. The primary features of this improved model are its capability to accurately resolve the electron motion and the enhanced field excitation source term. Similar to the classical codes, slow variables of both the field and motion are utilized to achieve comparable computational performance.

For demonstration, simulations of a coaxial cavity and an ideal second-harmonic case are presented. The improved model of ROCK shows greater accuracy in certain scenarios. The effects of these improvements will be examined against experimental data in more detailed future studies.

Author Contribution C.W. derived equations and methods, implemented numerical solvers, and wrote the main manuscript text; L.F. contributed to the justification of equations and methods, application programming, testing, validation, and prepared Fig. 4; A.S. contributed to application programming, testing, and validation; S.I. contributed to validation and prepared Fig. 4; M.T. provided scientific consulting and project oversight; J.J. provided project oversight and supervised the work; All authors reviewed the manuscript.

Funding Open Access funding enabled and organized by Projekt DEAL.

Data Availability No datasets were generated or analysed during the current study.

Declarations

Ethical Approval Not applicable

Conflict of Interest The authors declare no competing interests.

References

1. A. W. Fliflet, M. E. Read, K. R. Chu, and R. Seeley, "A self-consistent field theory for gyrotron oscillators: application to a low Q gyromonotron," *International Journal of Electronics*, vol. 53, no. 6, pp. 505–521, Dec. 1982. https://doi.org/b3kj5k
2. S. Y. Cai, T. M. Antonsen, G. Saraph, and B. Levush, "Multifrequency theory of high power gyrotron oscillators," *International Journal of Electronics*, vol. 72, no. 5-6, pp. 759–777, May 1992. https://doi.org/dv29fk
3. E. Borie, "Review of gyrotron theory," Kernforschungszentrum Karlsruhe, Tech. Rep. KfK 4898, Aug. 1991. https://doi.org/n7s8
4. S. Kern, "Numerische Simulation der Gyrotron-Wechselwirkung in koaxialen Resonatoren," ITP Forschungszentrum Karlsruhe, Tech. Rep. FZKA 5837, 1996. https://doi.org/n7s6
5. S. Alberti *et al.*, "Gyrotron parasitic-effects studies using the time-dependent self-consistent monomode code TWANG," in *International Conference on Infrared, Millimeter, and Terahertz Waves*. Houston, TX, USA: IEEE, Oct. 2011, pp. 1–2. https://doi.org/fx3jq3
6. K. A. Avramides, I. G. Pagonakis, C. T. Iatrou, and J. L. Vomvoridis, "EURIDICE: A code-package for gyrotron interaction simulations and cavity design," *EPJ Web of Conferences*, vol. 32, p. 04016, 2012. https://doi.org/gdvqdt
7. K. A. Avramidis, "Investigations and advanced concepts on gyrotron interaction modeling and simulations," *Physics of Plasmas*, vol. 22, no. 12, p. 123114, Dec. 2015. https://doi.org/f75jk4
8. G. N. Watson, *A treatise on the theory of Bessel functions*, 2nd ed., ser. Cambridge mathematical library. Cambridge: Cambridge University Press, 1995.
9. E. Borie *et al.*, "Mode competition using TE_{03} gyrotron cavities," *International Journal of Electronics*, vol. 72, no. 5-6, pp. 687–720, May 1992. https://doi.org/fsp2gv
10. J. P. Boris, "Relativistic plasma simulation-optimization of a hybrid code," in *Proceedings of the Fourth Conference on Numerical Simulation of Plasmas*. Naval Research Laboratory, 1970, pp. 3–67.
11. O. Buneman, "Time-reversible difference procedures," *Journal of Computational Physics*, vol. 1, no. 4, pp. 517–535, 1967. https://doi.org/dpkwjr
12. B. Piosczyk *et al.*, "A 1.5-MW, 140-GHz, $TE_{28\,16}$-coaxial cavity gyrotron," *IEEE Transactions on Plasma Science*, vol. 25, no. 3, pp. 460–469, 1997. https://doi.org/dh5g8d
13. C. J. Edgcombe, Ed., *Gyrotron oscillators: their principles and practice*. Washington, D.C: Taylor & Francis, 1993.
14. S. Illy, J. Zhang, and J. Jelonnek, "Gyrotron electron gun and collector simulation with the esray beam optics code," in *IEEE International Vacuum Electronics Conference*, 2015, pp. 1–2. https://doi.org/gdvqds
15. R. Holland, "Finite-difference solutions of Maxwell's equations in generalized nonorthogonal coordinates," *IEEE Transactions on Nuclear Science*, vol. 30, no. 6, pp. 4589–4591, Dec. 1983. https://doi.org/b5fkvq